01 Aug 2008

EMI Analysis Methods for Synchronous Buck Converter EMI Root Cause Analysis

David Pommerenke
Missouri University of Science and Technology, davidjp@mst.edu

Robert Steinfeld

Keong W. Kam

Cheung-wei Lam

Recommended Citation

D. Pommerenke et al., "EMI Analysis Methods for Synchronous Buck Converter EMI Root Cause Analysis," *Proceedings of the 2005 International Symposium on Electromagnetic Compatibility, 2008. EMC 2008*, Institute of Electrical and Electronics Engineers (IEEE), Aug 2008.
The definitive version is available at https://doi.org/10.1109/ISEMC.2008.4652125

EMI Analysis Methods for Synchronous Buck Converter EMI Root Cause Analysis

Keong W. Kam, David Pommerenke
Electromagnetic Compatibility Laboratory
Department of Electrical and Computer Engineering
Missouri University of Science and Technology
Rolla, Missouri, U.S.A

Cheung-Wei Lam, Robert Steinfeld
Apple Inc.
Cupertino, California, USA

***Abstract*— DC/DC synchronous buck converters cause broadband emissions. A variety of methods are applied to analyze the root cause of the EMI. Time-domain voltage measurement and joint-time-frequency analysis allows to determine the location of the noise source. The near field scan reveals the current paths, and impedance measurement and 3D modeling can be used for further analysis of the noise source. A dual port TEM cell allows to distinguish E from H field coupling, This paper shows the application of those methods to a synchronous buck converter and reveals the sources of EMI leading to advice on the optimal PCB design. Finally, an innovative method of using a TEM cell measurement to predict the maximum possible radiated emissions is introduced.**

Keywords- DC/DC synchronous buck converters; EMI; TEM cell

I. INTRODUCTION

Switched-mode power supplies are widely used in today's electronic systems because of their superior efficiency over linear power supplies. [1] However, switched-mode power supplies often cause EMI problems due to their nature of fast switching voltages (dv/dt) and currents (di/dt). [1] One of the most commonly used step down DC/DC converter topologies is the synchronous buck converter. The synchronous buck converter consists of two switches turning on and off alternatively and an inductor charging and discharging according to the switching state.

A variety of EMC analysis methods are applied to analyze the EMI behavior of such converter.

A 4-layer experimental test board containing a single synchronous buck converter was designed. The layout of the test board was drawn very similar to an evaluation board from a well known PWM controller vendor. The layer stack-up of the test board was the following:

- Layer 1: Signal (PWM Chip, Inductor, Bootstrap, Startup Circuit, etc.)
- Layer 2: Solid Ground Plane
- Layer 3: Ground Plane with 2 small islands for Vin, and Vout
- Layer 4: Signal (MOSFETs, Input Decoupling Capacitors)

Figure 1 shows the far-field radiated emission from the synchronous DC/DC buck converter on the 4-layer test board.

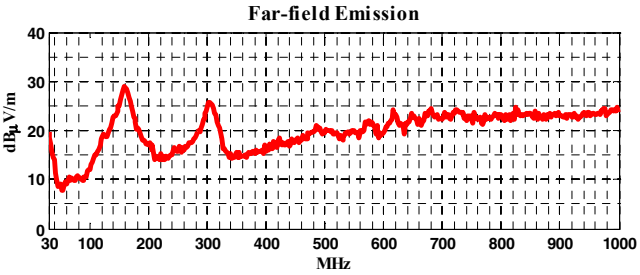

Figure 1. Far-field Emission of a Synchronous Buck Converter

The far-field measurement shows the broadband emission centered at around 160 MHz. This broadband emission in 100 – 200 MHz range is the main focus of this study.

In Sections II - IV, theoretical principles necessary to understand the root cause of the 160 MHz broadband noise are explained along with variety of measurement methods used to locate and understand the source of the noise.

Section V presents case study which shows that the loop inductance of the loop created by the input decoupling capacitor and the two MOSFETs affects the ringing frequency of the voltage at the phase node. Then, it is followed by Section VI which shows the connection between the resonance in the Decap-MOSFET loop and the far-field emission.

Section VII and VIII explains the method of using a TEM cell to quantify the board's ability to electrically and/or magnetically couple to surrounding structures. This method shows how the modifications made in Section V changed the magnetic coupling.

Finally, Section IX shows the implementation of an innovative method of using a TEM cell measurement to estimate the maximum possible far-field emission as explained in [7]. The significant is that the method was successfully implemented on a complex circuit system.

II. VOLTAGE MEASUREMENT

Figure 2 shows the schematic of the synchronous buck converter test board with parasitic elements when the high-side MOSFET is on, and the lows-side MOSFET is off.

978-1-4244-1699-8/08/$25.00 ©2008 IEEE

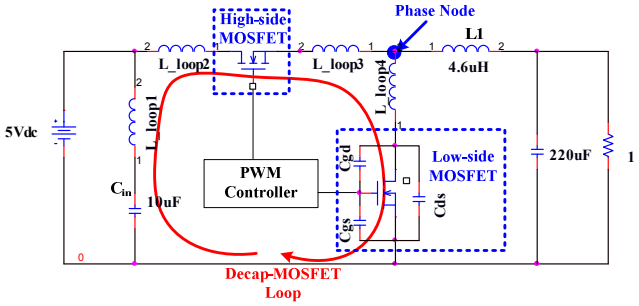

Figure 2. Synchronous Buck Converter with Parasitic Elements

Consider the case when the high-side MOSFET turns on and the low-side MOSFET turns off. The input decoupling capacitor and the two switching MOSFETs form a loop (Decap-MOSFET loop). The loop inductance of the Decap-MOSFET loop is represented as distributed partial inductances, L_{loop1}, L_{loop2}, L_{loop3} and L_{Loop4} shown in Figure 2. The low-side MOSFET can be modeled by capacitances C_{gd}, C_{gs} and C_{ds} when turned off. During the switch-on of the high-side MOSFET, the AC current is provided by the input decoupling capacitor, C_{in}. Although the low-side MOSFET is turned off, the total capacitance between drain and source of the low-side MOSFET allows the flow of the AC current. Because the output inductor L1 will have much higher impedance at high-frequency, one can expect that the AC current during switching mainly stays within the Decap-MOSFET loop.

The loop inductance of the Decap-MOSFET loop and the total capacitance between the drain and source of the low-side MOSFET (combination of Cgd, Cgs, and Cds) when turned off, will resonate at some resonant frequency, f_{res}. This resonant frequency causes the ringing on the voltage at the phase node. Figure 3 shows the measured voltage waveform at the phase node.

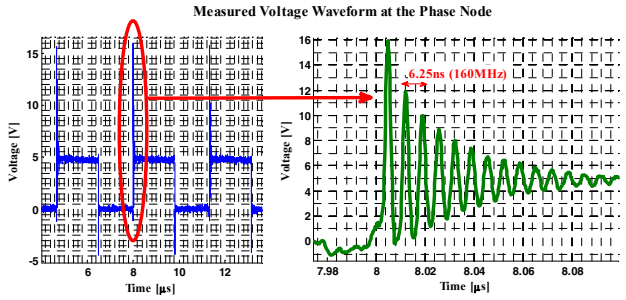

Figure 3. Measured Voltage Waveform at the Phase Node

STFFT (Short-Term FFT) of the time domain voltage waveform in figure 4 clearly shows the 160 MHz broadband component during the turning-on of the high-side MOSFET (rising edge of the phase voltage). This indicates that the resonance occurs when the high-side MOSFET turns on and the low-side MOSFET is off.

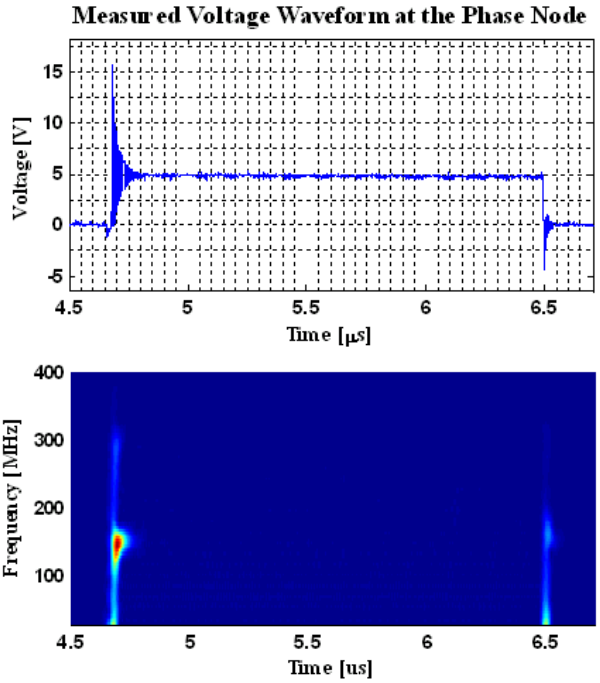

Figure 4. STFFT of the Measured Voltage Waveform at the Phase Node

The phase voltage measurement shows that there is a connection between the Decap-MOSFET loop resonance and the phase node voltage ringing frequency. One can also expect that this resonance in the Decap-MOSFET loop results significant amount of RF current especially at the resonant frequency, which can magnetically couple to nearby radiating structures such as large planes and cables, and cause radiated emission problems. Near-field measurement on the next section further proves that there is significant amount of noise current at 160 MHz flowing in the Decap-MOSFET loop.

III. Near-field Measurement Using Magnetic Loop Probe

Magnetic loop probes can be used to capture the magnetic flux generated by the current flowing in the system. [3] The voltage measured using the loop probe is therefore proportional to the time derivative of the current, which is proportional to the magnetic coupling. [4]

A 1mm x 1mm double loop probe as shown in figure 5 was placed so that the flux generated by the currents entering high-side MOSFET, low-side MOSFET, and the inductor, L1 can be captured by the probe. Figure 6 shows the spectrum of the measured signal using the loop probe.

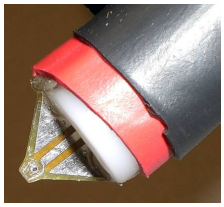

Figure 5. 1mm x 1mm Double Loop Probe used for Near-field Measurement

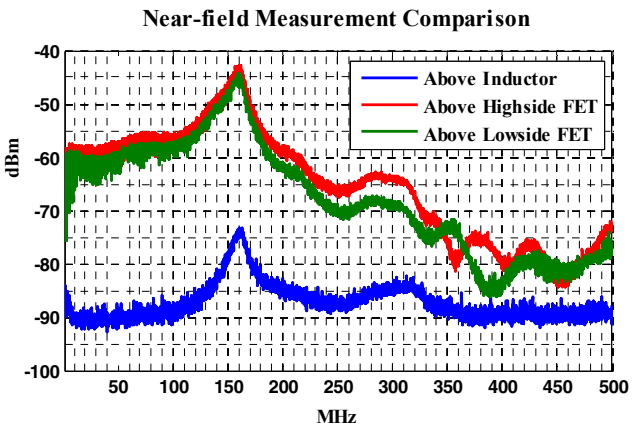

Figure 6. Near-field Measurement Comparison

As shown in Figure 6, at 160 MHz, the signal picked up by the loop probe at the high-side and low-side MOSFET shows much larger amplitude than that of L1. This suggests that most of the 160 MHz current stays within the Decap-MOSFET loop. Notice that the far-field spectrum shown in Figure 1 also shows a broadband emission centered around 160 MHz. The near-field measurement shows that the Decap-MOSFET loop contains significant amount of the 160 MHz current which is the result of the resonance due to the Decap-MOSFET loop inductance and the capacitance across the low-side MOSFET.

IV. Quantifying the Resonance at the Decap-MOSFET Loop

The resonance at the Decap-MOSFET loop is due to the loop inductance and the capacitance across the low-side MOSFET. Using a network analyzer, the impedance looking into the Decap-MOSFET loop was measured when the high-side MOSFET is on and the low-side MOSFET is off. The measured input impedance looking into the Decap-MOSFET loop is shown in figure 7.

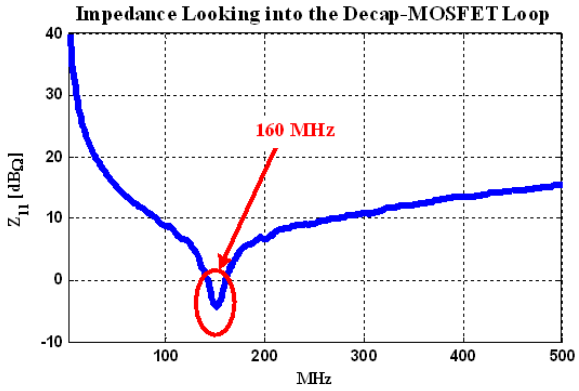

Figure 7. Impedance Looking into the Decap-MOSFET Loop

The measured impedance looking in to the loop shows that the loop resonates at 160 MHz.

To further quantify the components which contribute to the 160 MHz, first, the capacitance across the low-side MOSFET was measured using a network analyzer. The capacitance was measured with the low-side MOSFET turned off and 5V applied across the drain and source. The measured capacitance across the drain and source of the low-side MOSFET was about 210 pF.

Next, a 3D Passive simulation of the decap-MOSFET structure was performed using CST Microwave Studio (MWS). The exact geometry of the actual layout was drawn in the MWS as shown in figure 8. The 'ON' high-side MOSFET was modeled as an on-resistance with a series connection inductance. The 'OFF' low-side MOSFET was modeled as a 210pF capacitor as measured. The structure was simulated, and the loop inductance was calculated to be about 4.3nH.

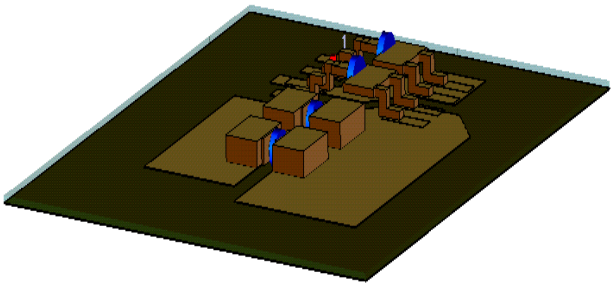

Figure 8. Decap-MOSFET Loop Modeled in MWS

The measured capacitance across the low-side MOSFET and the calculated loop inductance based on the geometry can be used to calculate the resonant frequency as following:

$$f_{res} = \frac{1}{2\pi\sqrt{L_{Loop} \cdot C_{MOSFET}}} = \frac{1}{2\pi\sqrt{(4.3nH)\cdot(210pF)}} = 167\,MHz$$

The calculated resonant frequency is fairly close to the measured resonant frequency.

V. Case Study: Effect of the Loop Size of the Decap-MOSFET Loop

The loop inductance of the decap-MOSFET loop and the parasitic capacitance across the low-side MOSFET forms a resonant structure. The resonant frequency determines the frequency of the current flowing in the loop. This noise current also causes voltage ringing at the phase node. The following case study shows the connection between the Decap-MOSFET loop size and the resonant frequency of the loop.

Three cases are examined as shown in Figure 9:

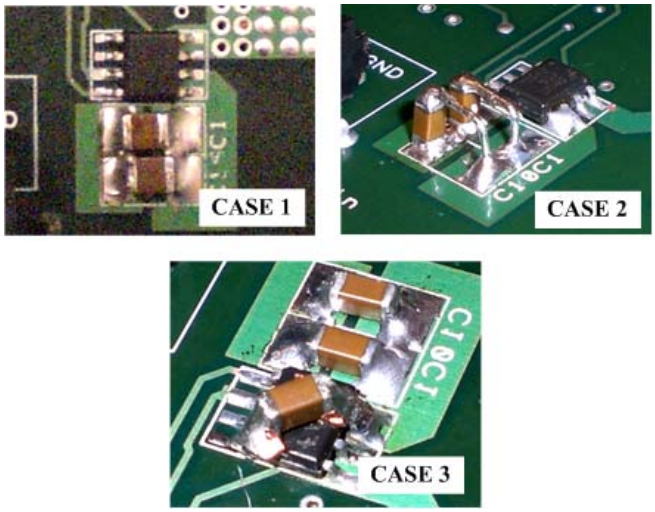

Figure 9. Three Cases Examined

The top left picture in Figure 9 shows Case 1, where the board is unmodified. Two input decoupling capacitors are placed right next to the dual MOSFET chip that contains the high- and low-side MOSFETs. The top right picture in Figure 9 shows Case 2, where the two input decoupling capacitors are modified to have a larger loop area. This makes the decap-MOSFET loop larger compared to Case 1, and thus, the loop inductance will also increase. The bottom picture in Figure 9 shows Case 3 where an extra decoupling capacitor is mounted directly across the chip between the drain pin of the high-side MOSFET and the source pin of the low-side MOSFET. This minimizes the size of the Decap-MOSFET loop, thereby reducing the loop inductance.

For the three cases above, one can expect a shift of resonant frequency as the loop inductance is changed. The voltage at the phase node was measured for each case to verify the change in ringing frequency. The ringing frequency was 160 MHz for Case 1, 130 MHz for Case 2, and 190 MHz for Case 3. As expected, the higher inductance in Case 2 shifts the ringing frequency down while the lower inductance in Case 3 shifts the ringing frequency up.

In Section III, it has been shown that the noise current due to this resonance primarily stays within the decap-MOSFET loop. One can expect that changing the size of this decap-MOSFET loop which carries a large amount of noise current will change the magnetic coupling due to flux wrapping from this loop. This will become more apparent in Section VII where TEM cell measurements show a decrease in magnetic coupling.

VI. FAR-FIELD MEASUREMENT

A standard 3m far-field measurement in a semi-anechoic chamber was performed for the three cases mentioned in Section V. Figure 10 shows the measured far-field spectrum for the three cases. For each case, the far-field measurement shows consistency between the ringing frequencies of the phase voltage and the peak frequency of the broadband emission. Notice that the far-field spectrum shows a peak at 160 MHz for Case 1, 130 MHz for Case 2, and 190 MHz for Case 3, which matches the ringing frequencies of the voltage measured at the phase node for each case. Also, notice that the up-shifted peak at 190 MHz in Case 3 shows a significant reduction in amplitude compared to that of Case 1. The down-shifted peak at 130 MHz in Case 2 shows larger amplitude than that of Case 1.

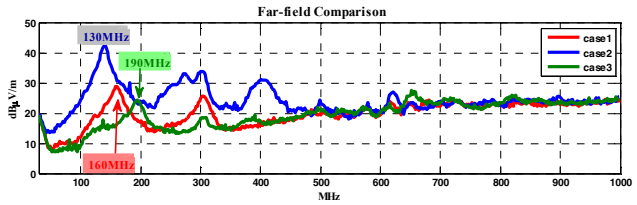

Figure 10. Far-field Spectrum for the Three Cases

This result demonstrates that the broadband emission at 160 MHz in the original case (Case 1) can be mitigated by minimizing the size of the decap-MOSFET loop. Reducing the loop size reduces the mutual inductance between the loop and the radiating structure (e.g. cables).

VII. TEM CELL MEASUREMENT

Previous work on electromagnetic compatibility (EMC) measurements of integrated circuits (ICs) shows that electric and magnetic coupling from ICs can be quantified using TEM cell measurements [5]. The device attached to a TEM cell electrically and/or magnetically couples to the septum inside the cell generating a TEM wave. Two ports of the TEM cell can be connected to a 180° hybrid to separate electric and magnetic coupling as shown in [5]. [6] describes how an electrically small radiating source inside a TEM cell can be characterized as an electric and/or magnetic dipole by measuring dipole moments based on TEM cell measurements which can then be translated into far-field estimation.

The buck converter test board used in the previous sections was used to perform a similar TEM cell measurement using a 180° hybrid.

The 10cm x 10cm buck converter test board was placed on the TEM cell. The board can be placed with the top or bottom layer facing down. For each side facing down, the board can be placed in one orientation (horizontal orientation), and then can be rotated by 90° for another orientation (vertical orientation). These two different orientations for each does not make a difference in E-coupling measurement, but is important for H-coupling measurement as the H-coupling changes depending on the direction of the current on the board.

A 180° hybrid was used to add and subtract signals from the two ports of the TEM cell to separate components due to E- and H- coupling as shown in figure 11. Figure 12 shows the comparison of measured H-coupling with the bottom layer facing down for Case 1 and Case 3 from Section V. The bottom layer of the test board contains the input decoupling capacitor and the switching MOSFETs.

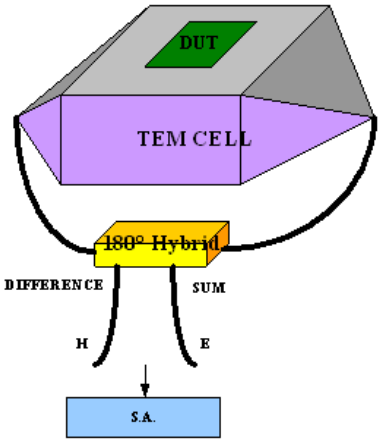

Figure 11. TEM Cell Measurement Setup

Comparing the results for the two cases, it is observed that the peak frequency has shifted from 160 MHz to 190 MHz. Also, it can be observed that the H-field coupling shows a 10dB reduction at the peak frequency comparing Case 3 to Case 1.

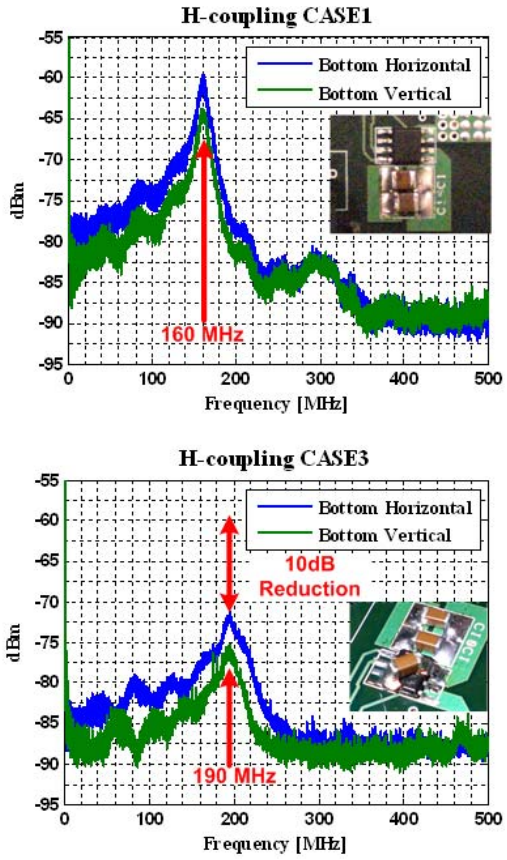

Figure 12. TEM Cell Measurement Results

The result again suggests that reducing the size of the Decap-MOSFET loop as explained in Section V reduces the magnetic coupling. Also, the reduction in magnetic coupling from TEM cell measurement coincides with reduction in Far-field emission. This indicates that the coupling path for the 160 MHz broadband noise which resulted in far-field emission was the magnetic coupling from the decap-MOSFET loop.

VIII. Reducing Exposed Phase Voltage Area

As shown in Section II, the voltage at the phase node contains high-frequency components indicated by the ringing frequency. Reducing the size of the exposed copper area which contains the phase voltage can reduce the E-coupling from this voltage. Figure 13 shows the modified version of the test board showing the reduction of the exposed phase voltage area.

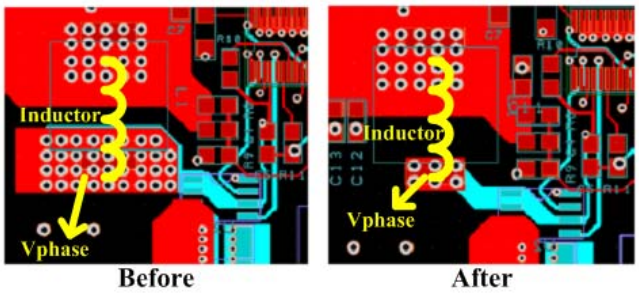

Figure 13. Reduction of the Exposed Phase Voltage Area

TEM cell measurement explained in Section VII was performed for the two cases to compare the E-coupling. Figure 14 shows the comparison of the measured E-coupling from the TEM cell measurement.

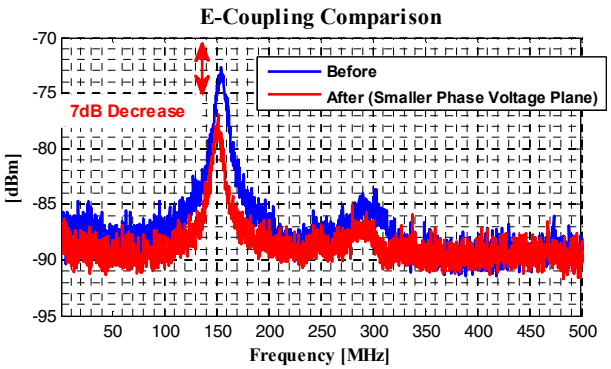

Figure 14. E-coupling Comparison of the Two Cases Shown in Figure 13

Figure 14 shows that after reducing the exposed phase voltage area, E-coupling decreased by about 5dB as expected.

However, the modification did not make any difference in far-field measurement. The case study in Section V has shown that the magnetic coupling from the Decap-MOSFET loop may be the dominating coupling mechanism that resulted the broadband emission at 160 MHz. And, the fact that this modification, although it decreased the E-coupling, did not affect the far-field emission further indicates that the dominating coupling mechanism was magnetic coupling for this particular case.

IX. Calculation of Maximum Possible Radiated Emission Due to Common Mode Current from the Magnetic Coupling Using TEM Cell Measurement

As explained in Section VII, the TEM cell measurement can be used to determine the DUT's ability to magnetically or electrically couple to the nearby structure. By separating E- and H-coupling component, one can determine matters such as which type of coupling results which frequency component. Measurement of H-coupling allows the calculation of mutual inductive coupling from the DUT, and one can calculate the common-mode voltage induced across the DUT, which can drive the antenna structure such as attached cables. [7] shows how the H-coupling measurement from the TEM cell measurement can be used to determine this common mode voltage induced across the DUT and to determine the maximum possible radiated emission due to this common mode voltage.

Using the method given in [7], the induced common-mode voltage (V_{CM}) on the board due to magnetic coupling was calculated based on the H-coupling measurement from the TEM cell. Then, the common mode voltage was used to determine the maximum-possible radiation at all frequency using the $\lambda/2$ dipole equation.

To verify the calculated maximum possible radiated emission, the far-field of the test board was measured with the board attached to the butterfly antenna shown in figure 15.

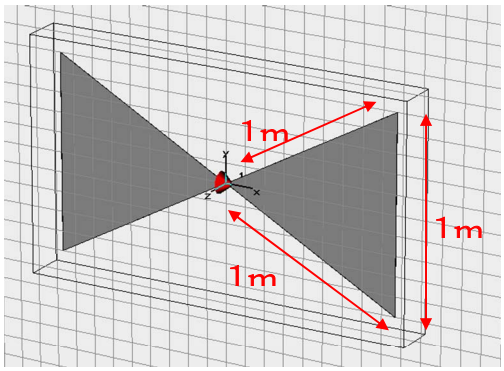

Figure 15. Butterfly Antenna Used for Far-field Measurement

Figure 16 shows the measured far-field without the butterfly antenna, measured far-field with the butterfly antenna attached, and the predicted maximum possible radiated emission using the TEM cell measurement.

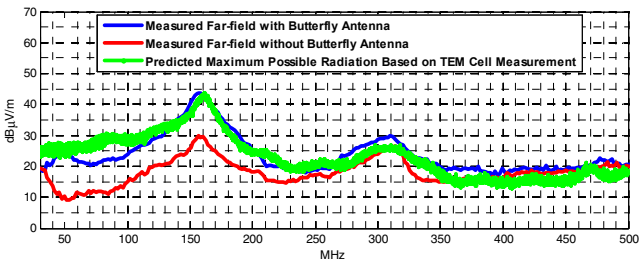

Figure 16. Comparison of the Measured Far-field vs. Predicted Maximum Possible Radiated Emission Using TEM Cell Measurement

Figure 16 shows that the measured far-field without the butterfly antenna is well below the predicted maximum possible radiated emission calculated using TEM cell measurement. Also, the far-field with the butterfly antenna, which is an efficient radiator in the above range of frequency, matches quiet well with the predicted maximum possible radiated emission. The reason for this good match is because the dominant radiation mechanism for this case was magnetic coupling, and the maximum possible radiated emission was calculated based on the magnetic coupling measured from the TEM cell.

X. Conclusion

The motivation of the presented study was to determine the source and coupling path of the low frequency broadband noise in a synchronous buck converter using a variety of EMC analysis methods.

The time-domain measurement of the phase voltage, and the joint-time-frequency analysis using STFFT showed that the 160MHz broadband component occurs during the turn-on of the high-side MOSFET.

Near-field measurements using a small magnetic loop probe revealed that the 160 MHz noise current is mainly within the Decap-MOSFET loop.

The resonant frequency calculated using the measured capacitance across the low-side MOSFET and the loop inductance of the Decap-MOSFET loop from the 3D simulation was close to 160 MHz.

Changing the size of the Decap-MOSFET loop had direct effect on the resonant frequency as the loop inductance is changed. Also, it was pointed out that reducing the decap-MOSFET loop size reduces mutual magnetic coupling between the source and the radiating structure, and thus results in reduction of far-field emission. The TEM cell measurement also indicates that the reduction in decap-MOSFET loop size reduced the magnetic coupling from the board.

It was shown through TEM cell measurement that reducing the size of the exposed phase voltage plane reduced the electric coupling resulting from the plane. However, the fact that the far-field emission didn't change indicates that the radiation was not strongly driven by electric coupling.

Finally, the maximum possible radiated emission due to magnetic coupling was approximated using TEM cell measurements as shown in [7]. This method seems to be quiet effective in predicting the worst-case scenario for radiated emissions.

REFERENCES

[1] M.H. Nagrial, A. Hellany, "EMI/EMC Issues in Switch Mode Power Supplies (SMPS)," 1999, EMC York 99, International Conference and Exhibition on Electromagnetic Compatibility (Conf. Publ. No. 464), Pages: 180 – 185.

[2] Zhe Li, David Pommerenke, "EMI Specifics of Synchronous DC-DC Buck Converters," 2005, EMC 2005, 2005 International Symposium on Electromagnetic Compatibility, Volume 3, 8-12 Aug. 2005 Pages: 711 – 714.

[3] Douglas C. Smith, “Signal and Noise Measurement Techniques Using Magnetic Field Probes,” 1999 IEEE International Symposium on Electromagnetic Compatibility, Volume 1, 1999 Pages: 559 – 563.

[4] C. Paul, Introduction to Electromagnetic Compatibility, New York: Wiley, 1992.

[5] V. Kasturi, S. Deng, T. Hubing, D. Beetner, “Quantifying Electric and Magnetic Field Coupling from Integrated Circuits with TEM Cell Measurements,” 2006, EMC 2006, 2006 IEEE International Symposium on Electromagnetic Compatibility, Volume 2, 14-18 Aug. 2006, Pages: 422 – 425.

[6] I. Sreenivasiah, D.C. Chang, M.T. Ma, “Emission Characteristics of Electrically Small Radiating Sources from Tests Inside a TEM Cell,” 1981, IEEE Transactions on Electromagnetic Compatibility, Volume: EMC-23, Issue: 3, Part I, Aug. 1981, Pages: 113-121.

[7] Shaowei Deng, “Innovative Applications of TEM Cell Measurements In Predicting Radiated Emission Due to Common-Mode Current on Printed Circuit Boards”, Dissertation, University of Missouri – Rolla, 2007